INSTITUTE FOR HIGH ENERGY PHYSICS

IHEP 94-24

V.V.Babintsev[1] , A..G.Kholodenko, Yu.V.Rodnov

SEVERAL VERSIONS OF FORWARD GAS IONIZATION CALORIMETER

[1]e-mail: babintsev@mx.ihep.su

Protvino 1994

UDK 539.1.01 M-24

Abstract

Babintsev V.V., Kholodenko A.G., Rodnov Yu.V. Several Versions of Forward Gas Ionization Calorimeter : IHEP Preprint 94-24. – Protvino, 1994. – p. 36, figs. 15, tables 7, refs.: 13.

The properties of several versions of a gas ionization calorimeter are analyzed by means of the simulation with the GEANT code. The jet energy and coordinate resolutions are evaluated. Some calorimeter versions meet the ATLAS requirements[1].

Аннотация

Бабинцев В.В., Роднов Ю.В., Холоденко А.Г. Некоторые варианты газового переднего калориметра : Препринт ИФВЭ 94-24. – Протвино, 1994. – 36 с., 15 рис., 7 табл., библиогр.: 13.

Анализируются некоторые варианты газового ионизационного калориметра посредством моделирования по программе GEANT. Получено координатное и энергетическое разрешение струй в переднем калориметре. Несколько вариантов переднего калориметра удовлетворяют требованиям ATLAS.

Introduction

One of the detectors of the future ATLAS set-up[1] is a forward calorimeter designated for the detection of the flow of particles originated from a primary interaction in the pseudorapidity range $3 < |\eta| < 5$. Several different projects of the forward calorimeter design are mentioned in the Letter of Intent[1]. High pressure gas ionization prototypes have been proposed among them[2-5]. It was observed that this kind of calorimeter type has good radiation resistance properties as well as sufficiently good energy resolution and can meet the ATLAS requirements. According to the requirements[1] imposed on the forward calorimeter its energy resolution has to be of the value

$$\frac{\sigma}{A} = \frac{100\%}{\sqrt{E}} \oplus 7\%.$$

The aim of the given article is to analyze the properties of some design versions of gas ionization calorimeters by means of simulations with the GEANT code[6]. The execution of the ATLAS requirements are checked out for the calorimeter versions which are similar in design to those proposed in [2].

1. The simulation conditions

The forward calorimeter is assumed to be located at a distance of 15.4 m from the central point of the ATLAS set-up and its total length cannot exceed 2.5 m. Therefore the radius R of the front calorimeter plane is about 1.5 m. The calorimeter volume is filled with cells. It is suggested that the cell cross section at the front calorimeter plane is about $10 * 10cm^2$. The simulated particle flow from the central point of the ATLAS set-up uniformly covers the same area on the calorimeter surface. The particle energy values is in the range (9-100) GeV.

To check out the possible coordinate dependence of the calorimeter properties the energy resolution of particles is calculated for two radii: $R \approx 35$ cm and $R \approx 105$ cm, where the radius R is determined in the front calorimeter plane. Incoming particles have two following angles to the beam line (Z-axis) in the radial plane (R-Z plane) for the chosen radii:

$$\theta \approx 1.2^0(\eta = 4.3) \text{ and } \theta \approx 5^0(\eta = 3.1).$$

The central part of the calorimeter has a hole with the radius R= 20 cm.

The simulations have been produced for gas ionization tubes filled up with the gas mixture ($90\%Ar + 10\%CF_4$) under the pressure of P= 30 atm. The influence of the electronic noise is not considered in this article. The carier drift distance in the gas gaps has to be about 2 mm to yield fast enough time response. Therefore, for example, the inner diameter of the gas ionization tubes used in some calorimeter versions is fixed at the value of 4 mm. The thickness of the iron tube wall is 1 mm. The tubes are oriented approximately along the direction of incoming particles forming definite angles to the Z-axis in the (R-Z) plane (radial plane). In the (X-Y) plane the tubes are situated at the vertices of an equilateral triangle with the side length L in the front calorimeter plane. The variety of the tubes in the (X-Y) plane can be arranged into parallel rows or concentric circles. According to the analysis made earlier the ratio of the gas volume to that of the calorimeter with gas ionization tubes can be about 10-25(%). That is why we will analyze here the tubes disposition with two values of the triangle side length L= 0.8 cm and L= 1.15 cm having the gas content 23% and 11%, respectively. The data for the intermediate cases can be obtained by linear interpolation in the gas content parameter.

Most amplitude distributions obtained for the analyzed calorimeter prototypes are not fitted to the Gaussian and we use here the RMS values of the histograms as the estimation of the amplitude dispersions. The energy resolution parameters are defined from the expression

$$\frac{RMS}{E} = \frac{A}{\sqrt{E}} \oplus C \qquad (1)$$

by approximating the simulated data. Instead of using fit procedure the constant term C of the energy resolution equation for hadrons can be evaluated with a sufficiently good accuracy from the expression (see references [5,7]):

$$C = (14 \div 25)\% * (\frac{e}{h} - 1).$$

For the simulation purpose lead or iron will be used in the calorimeter as an absorber. The quantitative difference of these two absorber materials is

seen from table 2, where the data are presented for the simulation of an ideal big calorimeter with a linear structure of the gas ionization tubes. (All tubes axes are parallel to the Z-axis and in the (X-Y) plane one can see the rows of tubes). The angle of incoming particles to the Z-axis is 5^0. One can see, that the difference in the value of the constant term C for the hadron showers can achieve 5% for these two absorbers.

Some comparisons of the simulation results with experimental data are given in Appendix 1 where the values of the GEANT3.15 parameters are fixed.

All calorimeter versions analyzed below could be divided into two groups according to their difference in the design properties and the way of the signal collection.

2. The first group of the calorimeters

The analyzed prototypes of this group contain gas ionization tubes inclined to the beam line in the (R-Z) plane. Besides, these tubes are disposed along circumferences in the (X-Y) plane therefore the distance between the tubes varies along the direction of incoming particles. This distance depends also on the calorimeter radius R in the (X-Y) plane and varies in the range $\pm 0.5mm$ around the given one. As the result the gas content varies with the calorimeter depth and the energy resolution of these calorimeters cannot be optimized entirely.

All these features are clearly seen for the following design version of the forward calorimeter.

2.1. Version 1 (The radial slope of the gas ionization tubes)

The suggested design version of the calorimeter contains tubes radialy inclined in the (R-Z) plane at the angle 5^0 to the vector from the central point of beam interactions, therefore the value of the slope angle of the tubes to the Z-axis of the ATLAS set-up increases with the calorimeter radius R. The absorber material is lead. The view of the calorimeter is presented in fig.2. The calorimeter is made of the cells with a fixed tube number. The thickness of the cell walls is 1 mm of the same absorber material.

It is important to have the constant slope angle of the tubes to the all incoming particles because of the strong dependence of the energy resolution of electromagnetic showers on the slope angle. At the same time for the thus radialy inclined tubes the distance L between them is growing with the calorimeter depth and achieves, for example, the value 2*L at the calorimeter back plane

for the tubes begining at the radius R= 15 cm in the front plane. (The initial value L= 0.8 cm is defined in the calorimeter front plane).

The simulation results of this design version show that the constant term in the energy resolution for electrons equals $C_e = 25\%$ instead of 15% as in the case of the simple linear version (see chapter 1). The same for pions is $C_\pi = 20\%$ instead of 2%. Other values of the slope angle of the tubes cannot improve the energy resolution significantly because of:

— the dependence of the energy resolution on the slope angle of the particles to the tube axes [3];

— the variation of the distance value between the tubes with the calorimeter depth.

To improve properties of the given prototype one has to split it into three or more independent parts. This results in the significant complication of the calorimeter design and the reduction of its effective length.

One can conclude that this version of the calorimeter design does not meet the requirements for a forward calorimeter (without partitioning it into several longitudinal sections).

2.2. Version 2 (Composite calorimeter)

The removal of the constant term in the energy resolution can be achieved chosing the tube slope angles greater than $15^0 - 20^0$[5]. It is obvious that such values of the slope angle can be realized only at a small calorimeter length. Therefore one can study a prototype which has a 16 cm long electromagnetic section ($\approx$ 25 rad. lengths in the lead absorber) and hadron calorimeter section. In the electromagnetic section of the prototype all gas ionization tubes have the same slope angle at the radial plane (R-Z) about 15^0 - 20^0 to the Z-axis. In the second section of the prototype all tubes have the same slope angle about 179^0 to compensate for the deviation of the tubes in the first section from the beam line (Z-axis). Both sections are separated by a 4 cm air gap. Each section consists of cells with the same number of tubes. The thickness of the cell walls equals 1 mm of the absorber material. The cross-sections of the prototype are presented in fig. 3. Lead is supposed to be used as an absorber material to reduce the constant term of the hadron energy resolution and to decrease the length of the electromagnetic part.

The full amplitude value of a signal is defined as the sum of the cells amplitudes with the corresponding weight factors for both calorimeter sections.

These weight factors are determined by the minimization of the following functional

$$F = \sum^{event} (E - \sum^{cells} (w_1 A_1^i + w_2 A_2^i))^2. \qquad (2)$$

A^i - the amplitude in the cell i and the section j, E- the energy of the incoming particles, w_j- weight factors. The minimization procedure has to be carried out at the energy of the incoming particles $E > 10$ GeV (for details see chapter 3).

The simulation results (table 3) show that the energy resolution strongly depends on the number of the tubes in a cell. The constant term in the energy resolution has a large value for electrons and practically does not depend on the calorimeter radius R. This constant term can be described by the sum of two parts where the first one is the contribution of the cell walls ($\approx 8\%$) and the second one is the contribution of the same effect as in the first calorimeter version.

The deficiency of the given prototype is the nonlinear response of the electromagnetic calorimeter part for $\gamma-$ rays owing to the large slope angle of the tubes. The position of the maximum energy release of the electromagnetic showers depends on the energy of incoming γ according to the expression

$$t(X_0) = ln(E/E_c) + 0.5,$$

where E_c- the critical energy of an absorber (E_c= 24 MeV for iron and E_c= 6.9 MeV for lead), E- the energy of incoming particles. Therefore the effective distance between the tubes becomes larger. The value of the nonlinearity achieves 12% for the energy range (9-100) GeV of the incoming particles. At the same time the nonlinearity for the pion amplitude response disappeares. The small dependence of the parameter C in the energy resolution on the calorimeter radius R for pions can be explained by a very small value of the slope angle of the tubes in the second section of the calorimeter. It is known that this dependence disappeares for the slope angle $\theta \approx 3^0$.

Therefore one can believe that this version will meet ATLAS requirements for a forward calorimeter at the following slope angles of the gas ionization tubes in two calorimeter sections

$$\theta_e \approx 15^0, \theta_h = 3^0.$$

3. The second group of calorimeter prototypes

This group contains prototypes where the gas content does not vary with the calorimeter length. If this kind of variations occurs then they take place only

between different calorimeter sections, and the full amplitude of a signal includes all changes by summing the weighted amplitudes. One of these versions, for example, has only 1 section.

3.1. Version 3 (Cells with parallel tubes)

The suggested calorimeter consists of the hexagonal cells with the outer diameter 9.6 cm (fig.4). Each cell consists of a lead absorber and rows of gas ionization tubes in the (X-Y) plane runing parallel to the beam direction. The thickness of the iron cell walls is 1 mm. To diminish the zero angle effect for the incoming $\gamma-$ rays there is a layer of lead situated at a distance of 50 cm before the prototype. The thickness of the layer is about 3 radiation lengths (2 cm). The purpose of the passive material is to create a flow of the secondary particles with wide angluar distribution to diminish the dependence of a signal value on the coordinate of the entry point of the incoming particles. There is also a constructive layer of iron 3 cm thick at a distance of 6 cm in front of the calorimeter.

From the simulation results presented in table 4 it follows that the energy resolution depends on the number of tubes in a cell. The constant term in the energy resolution for electrons is greater than 10% and depends on the entry point of the particles. This behavior can be explained by the energy resolution dependence on the incoming particles angle to the tubes axes[5]. The energy resolution for hadrons has a reasonable value but the amplitude ratio of electrons and pions depends on the entry point of the incoming particles into the calorimeter. As a result the jet energy resolution has to be depended on the entry point of the jet particles.

The ratio of normalized amplitudes A(100 GeV)/A(9 GeV) at two different energies deviates from 1 in the range $(9-16)\%$ for hadrons and in the range $(19-25)\%$ for electrons depending on the number of tubes in a cell.

One can conclude that this calorimeter type does not meet the ATLAS requirements.

3.2. Version 4 (Cells with gas chambers)

The volume of the suggested calorimeter prototype is filled with hexagonal cells (900 cells) which consist of the parallel absorber plates and gas ionization chambers. The latest achievements in obtaining fast signals from an ordinary layered structure of active and passive materials give the possibility of signal duration near 20 ns, as is necessary for the working conditions of the ATLAS set-up. In the basic variant the thickness of the iron cell walls is 2 mm. The

outer diameter of the cells is 9.6 cm. The width of the gas gap between the absorber plates is 4 mm. The induced charge in a cell is collected from 0.4 mm thick copper plates installed in the middle of the gas gaps. The calorimeter and cell cross-sections are presented in fig.5.

The variable parameters in the simulation are the material type of the absorber plates, their thickness, the thickness and material type of cell walls. Here we consider only those variants in which the type of the absorber material and the plate thickness are the same along the cell length.

The calorimeter has 3 longitudinal sections with the lengths 1λ, 2λ, 5λ (in the units of interaction length). The full amplitude value in a cell is calculated by summing amplitudes from these sections with the corresponding weight factors. These factors are determined through the minimization of a functional like functional (2).

It should be noticed that this minimization procedure gives biased results for low energy particles[7]. One can see the example of the energy dependence of the first two weighting factors in fig.6.

The simulation results are presented in table 5. The value of the constant term in the energy resolution equation for electromagnetic showers has a strong dependence on the thickness of the cell walls and the type of its material. In fig.7 one can see the amplitude distributions for the incoming electrons with the energy of E= 25 GeV. The influence of the wall material entirely disappears only for aluminium. Therefore the cell material has to be close to aluminium to improve the energy resolution for electromagnetic showers. The value of the constant term for hadrons is greater for the iron absorber plates as compared with lead ones. For lead absorber the amplitude ratio of electrons to pions is less than for the iron absorber.

The thickness of the absorber plates in the calorimeter has to be close to 2 cm rather than to 1 cm because the average energy leakage increases from $\approx 1\%$ to $\approx 2\%$ and the dispersion of the leakage distribution increases from 2% to 6% for the particles energy E= 100 GeV. (The energy leakage distribution for hadron showers has an exponential form). At the same time the thickness of the absorber plates has to be as small as possible because of the amplitude nonlinearity of signal for electromagnetic showers. Besides there is a constructive layer of passive material 3 cm thick before the calorimeter. The thickness of 2 cm for the absorber plates seems to be an optimal value.

The effective interaction length varies in the range (19-25) cm for the thickness of the absorber plates 2 cm. From the table it follows that the energy resolution does not depend on the calorimeter radius R.

According to the experimental data obtained for the TMP calorimeter [8] and the high pressure ionization calorimeter[4] interesting results have been obtained for the sampling calorimeter with the aluminum-clad absorber plates. In this case light material is used as a filter for slow electromagnetic particles and the difference between signal responses for hadrons and electrons decreases.

The similar structure was simulated here for each cell. The absorber plate, with the total thickness of 2 cm, consists of a lead plate (1.6 cm) covered with the aluminum plates 0.2 cm thick. One can see from the data that the parameter C for this calorimeter structure has the smallest values. The only disadvantage is the large value of the effective interaction length (λ = 26-32 cm). Therefore with the presence of the aluminum material in the calorimeter it is necessary to increase the thickness of the absorber plates or the total calorimeter length for this calorimeter type.

When each cell is used as a whole, without longitudinal partition, then in the case of the iron absorber plates the amplitude nonlinearity for hadrons is about 15% (the deviation of the ratio A(9 GeV)/A(100 GeV) from unity for normalized amplitudes A). The same for the lead absorber plates is 9%. In the case of the longitudinal cell partition these nonlinearities have to be less because of the calibration procedure.

One can make a conclusion that some variants of this calorimeter type meet the ATLAS requirements.

3.3. Version 5 (Hybrid calorimeter)

The next version of the forward calorimeter is a hybrid one. In this version each cell consists of two parts. The first one containes parallel ionization chambers interlived with the absorber plates and the second one consists of gas ionization tubes parallel to the beam direction. Each cell has a hexagonal shape with the iron wall thickness 2 mm. The outer diameter of the cell is 9.6 cm with the common gas filling in both parts. The width of the gas gap between the absorber plates in the first cell section equals 4 mm, and the induced charge is collected here by 0.4 mm copper plates installed in the middle of the gaps. The thickness of the iron absorber plates is chosen to be 2 cm. The calorimeter and cell cross-sections are presented in fig.8.

For the simulation purpose lead is used as an absorber material in the second cell section and in the first cell section it will be either lead or iron. Therefore the variable parameters in the simulation are the material type of the absorber plates in the first section of cells, the number of the absorber plates and the

number of ionization tubes in the second cell section. One can see the effect of the absorber plate thickness in the previous chapter.

The full amplitude from each cell is defined by the sum of 2 amplitudes with the corresponding weight factors, determined from the minimization of functional (2).

The investigation of this calorimeter type was carried out in two stages. First of all it is necessary to determine the length of the layered structure in each cell. It can be done through the determination of the minimal values of the energy resolution parameters for hadrons.

In fig.9 one can see the dependence of the parameters A and C from expression (1) on the length of the layered cell section in the unit of the interaction length. Two calorimeter types were simulated. The first one - with lead absorber in both cell sections and with 127 tubes in the second cell section (L= 0.8 cm), and the second one - with an iron absorber in the first cell section and with 91 tubes in the second cell section (L= 0.97 cm). From fig.9 it follows that the parameter C takes the minimal value at the length 2.5 λ.

The second stage of the investigation is carried out for this length of the first section in cells. The results of simulations are presented in table 6. The presence of the large constant term for electrons has the same nature as in the previous calorimeter version 4. The energy resolution for hadrons for the calorimeter variants with 127 tubes (L= 0.8 cm) in each cell has the same average value as in the previous calorimeter version, but the constant term is greater for this version in the case when there are 61 tubes (L= 1.15 cm) in a cell. From the table one can see that the energy resolution does not depend on the calorimeter radius R. In the table there are also the data for the variant where the stainless tubes of the outer radius 0.8 cm and with the iron rod inside is used. The rod diameter is 0.4 cm and the tube wall thickness is 0.05 cm. The distance between these tubes is L= 1.15 cm and there are 61 tubes in a cell. One can see that for this variant the energy resolution is practically of the same value as in the case of the ordinary tubes with the distance between them L= 0.8 cm (127 tubes in cell).

For those variants where aluminium hexagonal cells and lead absorber plates between aluminium sheets (thickness 2 mm) are used we have the smallest value of the constant term in the energy resolution. To the top of that if aluminium tubes instead of stainless ones are used the energy resolution does not change but we have a large value of the energy leakage. One can make a conclusion that for this calorimeter version aluminium can be used only in the first section of the cells. To decrease the energy leakage it is necessary to decrease the number of tubes in each cell.

The estimated amplitude nonlinearity is of the same value as in the case of the previous version.

One can make a conclusion that some variants of this calorimeter type meet the ATLAS reqirements[1].

4. Coordinate resolution

The coordinate resolution of the forward calorimeter for a single particle can be estimated with the help of the calorimeter design of version 4. As a rule some methods are used for this purpose [9]. They are all based on the definition of the coordinate as

$$< x >= \frac{\sum x_i * A_i}{\sum A_i}, \tag{3}$$

where A_i- the measured amplitude in the cell i, x_i- its coordinate. For a hadron shower this estimation is quite sufficient. However for electromagnetic showers this definition contains a systematic error, determined by the large cell size compared with the transverse size of an electromagnetic shower.

For this calorimeter version the coordinates dependences determined by expression (3) on the true coordinates are presented in fig.10 for the incoming particle energy E= 25 GeV. As it follows from the figure there is practically a linear relation between calculated and true coordinates for hadrons. For electromagnetic showers this dependence has a complicated structure, which can be explained by the hexagonal shape of the cell.

The methods of the coordinate estimations with the ratio of amplitudes in adjacent cells as a parameter are not applicable here because of the hexagonal cell shape. Consequently, we use here the method of approximating the deviation between the calculated and true coordinates by different functions. The parameters of the functions are determined through the minimization procedure of the functional

$$FF = \sum_{i}^{event} (x_i - f(< x_i >, A))^2, \tag{4}$$

where x_i- true coordinate of the particle entry point into the calorimeter, f- a function, depending on the variable $< x_i >$ and parameters A.

It is necessary to mention that because of the long length of hadron showers and the presence of their initial slope angle the reconstructed coordinates of particles are shifted from the true ones. For example, even for the calorimeter radius R= 30 cm (the slope angle of particles $\theta = 1.2^0$) with the incoming hadrons in energy increasing from 2 GeV to 25 GeV the overestimation of the reconstructed radius increases from 0.6 cm to 1.7 cm. To diminish the systematic

shift it is convenient to proceed to the polar coordinates r and ϕ. A reasonable coordinate reconstruction here is achieved with the following functions

$$\phi_{corr} = < \phi > + a * arctg\Big(\frac{\phi_{cell} - < \phi >}{c}\Big), \quad (5)$$

$$r_{corr} = < r > + a * \sin\Big(\frac{R_{cell} - < r >}{c}\Big) * \exp\Big(-\frac{|R_{cell} - < r > |}{d}\Big), \quad (6)$$

where the coordinates $< \phi >$ and $< r >$ are defined with expression (3). For a hadron shower, with account of the position of the maximum energy release and the distance of the calorimeter from the interaction point L, the radius is corrected as follows

$$< r >= \frac{\Sigma(w_i * R_i) * A_i}{\Sigma A_i},$$

$$w_i = 1.0 - \lambda * (0.7 + 0.2 * ln(E))/L.$$

A_i- the cell amplitudes and R_i- the radius of the central point in the cell i. As a result, the reconstructed radius for hadron is the same in fact as the true one.

The parameters of these functions depend on the particle energy. The energy dependence of the finally corrected coordinate standard deviation can be described as follows

$$\sigma_{\phi,r} = \frac{A}{\sqrt{E}} + B, \quad (7)$$

where the estimations of the parameters A and B are presented in table 7. In the case of a calorimeter with an iron absorber the reconstructed value R has to be corrected also for electromagnetic showers because of large shower lengths in iron.

It is necessary to mention that these calculations have been made for a single particle. In our case, when the forward calorimeter measures the jet energy with a large number of particles, we can use the expression (3) only. The accuracy of the jet coordinate resolution depends on the number of included cells and number of particles in jet. There is a full analogy with the coordinate resolution for hadron showers, and the final coordinate resolution for jets cannot be worse than for hadrons in the case of good coordinate resolution for electrons.

5. Discussions

Five different versions of a forward calorimeter have been analyzed. Only 3 versions meet the ATLAS requirements. Among them the composite calorimeter has a more complicated structure than the last two versions. Therefore the

sampling calorimeter version and the hybrid one can be considered as the basic versions of a forward calorimeter.

The cell size $\approx 10*10cm^2$ in the field of variables η and ϕ corresponds to the values $\Delta\eta * \Delta\phi \approx 0.1 * 0.1$ at the calorimeter radius R= 1.5 m and $\approx 0.5 * 0.5$ for R= 0.2 m. To evaluate the contribution of each cell into the P_T distribution there were simulated MINIBIAS and 2-jet events with the PYTHIA code[10]. To reproduce the experimental multiparticle distributions[11] the simulation was done with the presence of multiple interactions.

The dependence of the number of incoming particles and their mean P_T value in the calorimeter cells (without calorimeter simulation) on the calorimeter radius R for 10 MINIBIAS events is presented in fig.11. One can see a large difference in the load of cells. For 10 MINIBIAS events the full energy value deposited in the forward calorimeter in the range $3 < \eta < 6$ equals 5.0 TeV and 2.2 TeV in the range $3 < \eta < 5$. The same distributions are given for 2-jet events for jet particles. The 2-jets events were simulated using 40 GeV P_T-cut. Jets of 0.5 radius in the ϕ, η plane and $P_T(jet) > 20$ GeV were taken. It follows from the figure that the distributions for MINIBIAS events are steeper than those for 2-jet events. Taking into account the presence of background particles in jets from soft interactions one can suppose the distribution of jet particles over the forward calorimeter be approximately uniform. It means that the constant cell size along the calorimeter radius R is adequate for jet detection, when the jet definition is corrected for the forward calorimeter.

In fig.12 one can see the effect of the given cell size, where the distribution of difference for the initial $P_T(jet)$-value and detected one

$$|\Delta\vec{P}_T| = |\vec{P}_T(jet) - \vec{P}_T^{\,meas}(jet)|$$

are given for MINIBIAS jets with the jet energy E= 400 GeV and for jets with the energy E= 250 GeV from 2-jet events. Here $\vec{P}_T^{\,meas}(jet)$ is the total measured $\vec{P}_T(jet)$ value of a jet after the simulation of the forward calorimeter. (Versions 4 and 5 were used). The MINIBIAS jets are defined as the flow of particles, where entry points of particles occure in the calorimeter radius range $25 < R < 120(cm)$ of the front plane (with the aim to reduce the energy leakage). The same restriction has been used for 2-jet events. When we use a calorimeter a the small cell size 4.3*4.3 cm^2 we obtain the improvement in the $\phi-$ resolution of about 15% and in the R- resolution - about 5% fo r pions. As the result the $P_T(jet)-$ resolution as compared with that presented in fig.12, does not practically change. Therefore the $P_T(jet)-$ resolution in our case is entirely determined by the particle energy resolution of the calorimeter only.

The energy distributions of incoming particles for MINIBIAS and 2-jet events in the forward calorimeter ($3 < \eta < 5$) are presented in fig.13. As it follows from this figure the mean particle energy is far less than 100 GeV. It means that the stochastic term in the energy resolution can be more important for the jet energy measurement than the constant term if it is sufficiently small (see below). The energy of γ–rays is in average less than 10 GeV. For this energy range a great fraction of the particle energy is absorbed in passive layers before the first active layer. That is why the $P_T(jet)$– resolution of the calorimeter does not practically depend on the cell size.

According to the simulated and experimental data the energy resolution of jets may be considerably better than the single-pion one[12] because of a rather large fraction of e.m. energy. In this case the energy resolution of the forward calorimeter for a single hadron can be considered as an upper value for the jet energy resolution. In the first approximation order the jet energy resolution can be evaluated through the single particle resolution. For example, in average the number of γ–rays equals the number of hadrons in a jet. Therefore the average energy of γ–rays equals $E_\gamma = 1/3 * E * (1/N)$, where E- the energy of the jet and N- number of γ–rays or hadrons. The average energy of one hadron is $E_h = 2/3 * E * (1/N)$. Taking into account expression (1) the jet energy resolution can be expressed as follows:

$$\frac{\sigma_j}{E} = \sqrt{\frac{(2/3)A_\pi^2 E + (1/3)A_e^2 E + (4/9)C_\pi^2 E^2/N + (1/9)C_e^2 E^2/N}{E}}.$$

In the first approximation order one can believe that the number of particles in jets can be expressed as follows

$$\frac{3}{2}N = \frac{E}{k},$$

where k is a calibration factor. As the result we obtain that the jet energy resolution has no constant term, and the stochastic term of a jet is evaluated as follows

$$A_j \approx \sqrt{(2/3)A_\pi^2 + (1/3)A_e^2 + (3/2)k(4/9)C_\pi^2}$$

and the rough estimation of the k-factor is about 10-20. From this expression it follows that the hadron constant term determines the large fraction of the jet energy resolution.

To check this conclusion the MINIBIAS jets with different jet-energies have been simulated. The energy resolution of these jets was determined both for the calorimeter with layered structure of cells (version 4) and iron absorber plates (2 cm) and for the hybrid calorimeter with iron absorber plates (2 cm) and

with 91 tubes in each cell. Besides there is an iron constructive layer 3 cm thick before these calorimeters. The thickness of iron cell walls is 2 mm. The energy resolution data for jets and a single pion are presented in fig. 14. One can see, that the jet energy resolution is much better than the same for a single pion, but the stochastic term for jets is larger than for a single pion because of the large value of the constant term C. The jet energy resolution can be expressed in the following form:

for the iron sampling calorimeter

$$\left(\frac{\sigma}{A}\right)_{jet} = \frac{(85.0 \pm 3.0)\%}{\sqrt{E}} \oplus (2.8 \pm 0.8)\%$$

and for the hybrid one

$$\left(\frac{\sigma}{A}\right)_{jet} = \frac{(97.7 \pm 3.3)\%}{\sqrt{E}} \oplus (3.2 \pm 0.7)\%.$$

For a single pion the data can be taken from tables 5 and 6. It is necessary to mention that this energy resolution has been obtained for the case when there were 3 calorimeter longitudinal sections (1λ, 1.5λ, 5.5λ) for version 4 and with 2 longitudinal sections for the hybrid version. In the case without any longitudinal partition the stochastic term increases by $\approx 10\%$ for the sampling calorimeter and by $\approx 5\%$ for the hybrid calorimeter. The constant term is of the same value. The possible influence of the endcap criostat used in the ATLAS set-up is analyzed in Appendix 2.

The coordinate jet resolution in the ϕ and R variables can be expressed for version 4 in the form:

$$\sigma_\varphi = \frac{(1.10 \pm 0.30)}{\sqrt{E}} + (0.04 \pm 0.02)(rad),$$

$$\sigma_R = \frac{(15.1 \pm 1.5)}{\sqrt{E}} + (0.4 \pm 0.1)(cm).$$

And in the X,Y variables

$$\sigma_{X,Y} = \frac{(25 \pm 3)}{\sqrt{E}} + (0.6 \pm 0.2)(cm).$$

The average deviation value from zero for the resolution of the calorimeter radius R is about 2 cm. Approximately the same values have been obtained for the hybrid version. If we compare these coordinate resolution values with those from table 7, then we can make a conclusion that the coordinate resolution for a

single pion is better than for jets because of the bad electromagnetic coordinate resolution.

Taking into account all these data one can make a conclusion that practically all calorimeter variants of versions 4 and 5 meet the ATLAS requirements[1].

In conclusion we would like to thank F. Carminati, A. Dell'Acqua and S. Giani for their help in solving some problems in programs, connected with the GEANT code.

Table 1. Comparision of experimental data with the simulated ones , obtained for different values of GEANT parameters, for the sampling uranium calorimeter with gas proportional chambers (top part of the table). R- the energy resolution of E= 6 GeV pions. π/e- is the amplitude ratio. In the bottem part of the table there are results for high-pressure gas calorimeter with uranium and iron absorber plates. The energy of particles is E= 20 GeV.

	Exper. data	LOSS=2 HADR=3	LOSS=1 HADR=3	LOSS=2 HADR=1	LOSS=2 HADR=4
R_π	32.0 ± 1.0	31.1 ± 2.0	28.6 ± 0.8	30.2 ± 1.2	23.3 ± 0.9
π/e	0.79 ± 0.02	0.80 ± 0.01	0.70 ± 0.02	0.86 ± 0.01	0.98 ± 0.02
R_π	17.0	15.3 ± 2.1	15.0 ± 2.0	16.5 ± 2.5	13.5 ± 2.5
e/π	1.17 ± 0.03	1.21 ± 0.02	1.28 ± 0.02	1.16 ± 0.02	1.00 ± 0.02

Table 2. The dependence of the energy resolution parameters A and C from expression (1) on the absorber type, the side length L of the triangle forming the line structure of the gas tube disposition in an ideal big calorimeter. The direction of incoming particles makes the angle 5^0 to the tubes axis. The last column of the table presents the amplitude ratio for electrons and pions at E= 75 GeV.

Absorber type	L cm	e $A(\%)$	e $C(\%)$	π $A(\%)$	π $C(\%)$	e/π
Pb	0.8	46 ± 1	15 ± 1	70 ± 10	2.5 ± 0.5	1.06 ± 0.01
Fe	0.8	47 ± 2	3 ± 1	55 ± 10	7 ± 2	1.17 ± 0.01
Pb	1.15	91 ± 20	40 ± 5	114 ± 6	1 ± 1	1.03 ± 0.03
Fe	1.15	77 ± 10	19 ± 13	83 ± 10	8 ± 2	1.16 ± 0.02

Table 3. Version 2. The dependence of the energy resolution parameters A and C from the expression (1) on the calorimeter radius R and the distance L between the tubes. The two last columns of the table present the amplitude ratio for electrons and pions at E= 100 GeV and the average energy leakage with the dispersion of the energy leakage distribution.

R	L	e	e	π	π	e/π	Leakage
cm	cm	A(%)	C(%)	A(%)	C(%)		(%)
30	0.8	39 ± 2	15 ± 1	77 ± 2	11 ± 1	1.19 ± 0.02	1.2 ± 4.4
30	1.15	76 ± 3	21 ± 1	107 ± 3	19 ± 1	1.17 ± 0.02	0.7 ± 1.2
105	0.8	39 ± 2	15 ± 1	75 ± 2	9 ± 1	1.15 ± 0.02	1.2 ± 4.9
105	1.15	72 ± 2	18 ± 1	107 ± 3	12 ± 1	1.08 ± 0.02	0.7 ± 1.0

Table 4. Version 3. The dependence of the energy resolution parameters A and C from expression (1) on the calorimeter radius R and the distance L between the tubes. The two last columns of the table present the amplitude ratio for electrons and pions at E= 100 GeV and the average energy leakage with the dispersion of the energy leakage distribution.

R	L	e	e	π	π	e/π	Leakage
cm	cm	A(%)	C(%)	A(%)	C(%)		(%)
30	0.8	83 ± 4	16 ± 1	92 ± 3	9 ± 1	1.14 ± 0.02	1.2 ± 3.7
30	1.15	90 ± 8	30 ± 1	113 ± 5	17 ± 2	1.31 ± 0.02	0.6 ± 0.6
105	0.8	69 ± 4	11 ± 1	85 ± 3	9 ± 1	0.98 ± 0.02	0.9 ± 2.5
105	1.15	78 ± 7	23 ± 1	116 ± 3	15 ± 1	1.17 ± 0.02	0.7 ± 0.8

Table 5. *Version 4.* The dependence of the energy resolution parameters A and C from expression (1) on the calorimeter radius R, the width of absorber plates Δ and the absorber type. The last column of the table presents the amplitude ratio for electrons and pions at E= 100 GeV and the average hadron energy leakage with the dispersion of the energy leakage distribution. d- the width of cell walls in mm with its material type. The line marked with the asterisk presents results for the calorimeter structure, where the absorber plates consist of lead and aluminum material (see the text).

Absorber type	R cm	Δ cm	e $A(\%)$	e $C(\%)$	π $A(\%)$	π $C(\%)$	e/π (leakge %)
Pb d(Fe)= 2	30	2.0	40 ± 1	12 ± 1	93 ± 3	8 ± 1	1.28 ± 0.01 (0.9 ± 2.0)
Fe d(Fe)= 2	30	2.0	32 ± 1	12 ± 2	65 ± 3	11 ± 1	1.33 ± 0.01 (0.9 ± 1.8)
Pb d(Fe)= 2	30	1.0	26 ± 4	13 ± 1	67 ± 2	9 ± 1	1.29 ± 0.01 (1.6 ± 7.8)
Fe d(Fe)= 2	30	1.0	21 ± 1	13 ± 1	49 ± 3	13 ± 1	1.34 ± 0.01 (1.7 ± 5.6)
Fe d(Fe)= 1	30	2.0	26 ± 2	7 ± 1	67 ± 3	11 ± 1	1.34 ± 0.01 (1.3 ± 5.1)
Fe d(Al)= 2	30	2.0	29 ± 1	5 ± 1	74 ± 3	10 ± 1	1.30 ± 0.01 (1.5 ± 6.2)
*(Pb+Al) d(Al)= 2	30	2.0	37 ± 1	4 ± 1	86 ± 3	5 ± 1	1.20 ± 0.01 (1.4 ± 3.9)
Pb d(Fe)= 2	105	2.0	41 ± 3	9 ± 1	90 ± 3	8 ± 1	1.30 ± 0.01 (0.7 ± 1.7)
Fe d(Fe)= 2	105	2.0	31 ± 3	11 ± 1	65 ± 3	11 ± 1	1.32 ± 0.01 (0.9 ± 2.5)

Table 6. Version 5. The dependence of the energy resolution parameters A and C from expression (1) on the calorimeter radius R, the distance between the tubes and the absorber type in the first part of cells. The last column of the table presents the average hadron energy leakage with the dispersion of the energy leakage distribution at E= 100 GeV. The width of iron cell walls is 2 mm. The line marked with the word 'Rod' presents results for the calorimeter structure, where instead of ordinary tubes those ones with iron rods inside are used (see the text). The line marked with one asterisk presents results for the calorimeter structure, where the absorber plates consist of lead and aluminium material (see the text). The line marked with two asterisks has the same meaning as the previous one but with aluminium tubes instead of iron ones.

Absorber type	R cm	L cm	e $A(\%)$	e $C(\%)$	π $A(\%)$	π $C(\%)$	leakage (%)
Pb	30	0.8	40 ± 1	12 ± 1	86 ± 2	8 ± 1	0.9 ± 2.2
Fe	30	0.8	32 ± 1	12 ± 2	76 ± 3	11 ± 1	1.0 ± 1.8
Fe	30	0.97	36 ± 3	11 ± 1	68 ± 3	12 ± 1	1.0 ± 3.5
(Rod)Fe	30	1.15	36 ± 3	11 ± 1	65 ± 2	13 ± 1	0.9 ± 1.6
Pb	30	1.15	40 ± 1	12 ± 1	92 ± 2	13 ± 1	0.8 ± 2.0
Fe	30	1.15	32 ± 1	12 ± 2	71 ± 4	16 ± 1	0.7 ± 2.0
(*)(Pb+Al)	30	0.8	39 ± 1	4 ± 1	86 ± 5	6 ± 2	1.7 ± 6.0
(**)(Pb+Al)	30	0.8	39 ± 1	4 ± 1	84 ± 3	9 ± 1	3.0 ± 10.0
Pb	105	0.8	41 ± 3	9 ± 1	82 ± 2	9 ± 1	1.1 ± 4.6
Fe	105	0.8	31 ± 3	11 ± 1	70 ± 2	10 ± 1	1.0 ± 2.2

Table 7. The dependence of the coordinate resolution parameters A and C from expression (9) on the calorimeter radius R (version 4) for variables ϕ and r.

R cm	Variable	e A	e B	π A	π B
30	ϕ(rad.)	0.07	0.05	0.13	0.09
	r(cm)	1.4	0.8	2.3	1.6
105	ϕ(rad.)	0.04	0.02	0.11	0.02
	r(cm)	1.00	1.60	1.60	2.32

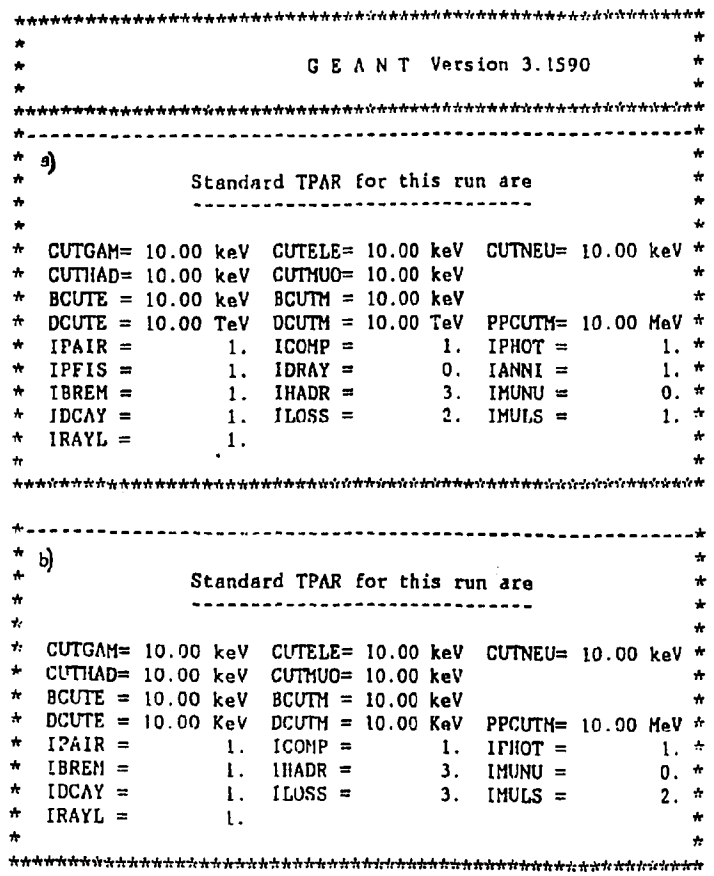

Fig. 1. Two sets of parameters values for simulation on the program GEANT3.15.

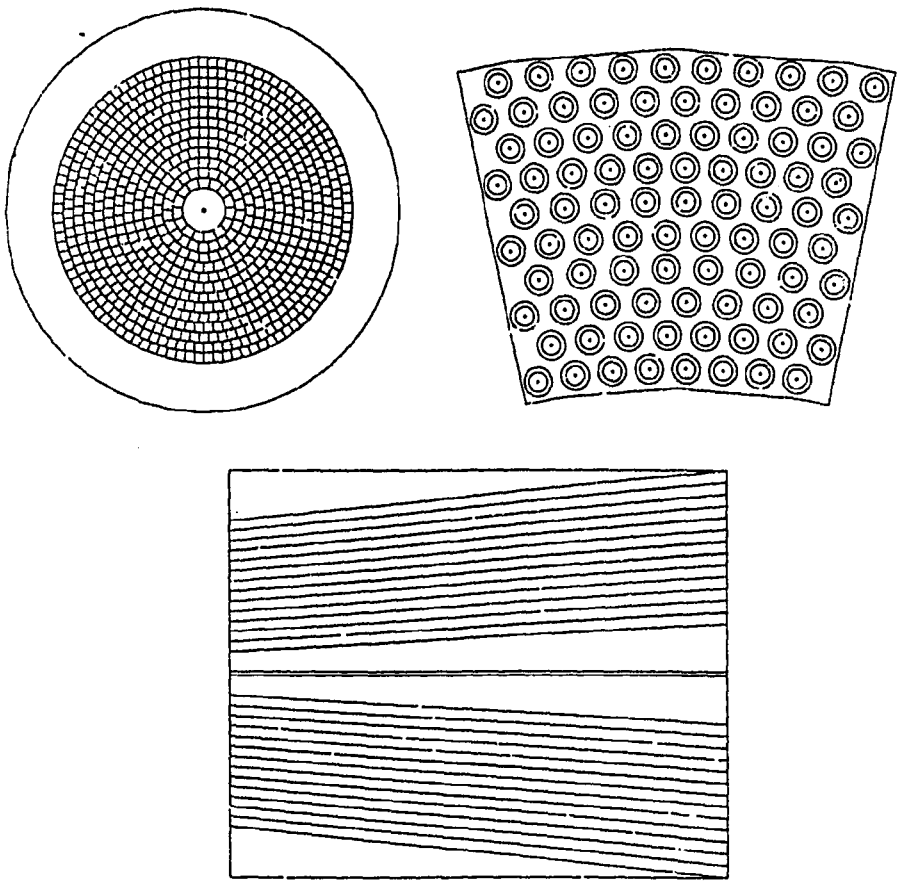

Fig. 2. Version 1. At the top part of the figure there are the calorimeter cross-section and the cell cross-section. At the bottom part of the figure there is the longitudinal section of the calorimeter.

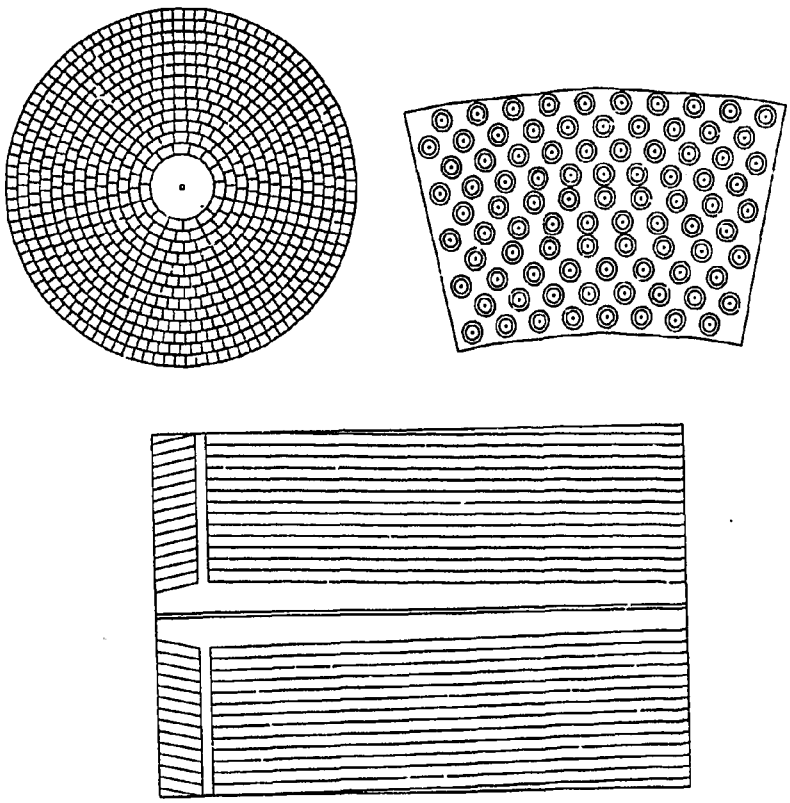

Fig. 3. Version 2. At the top part of the figure there are the calorimeter cross-section and the cell cross-section. At the bottom part of the figure there is the longitudinal section of the calorimeter.

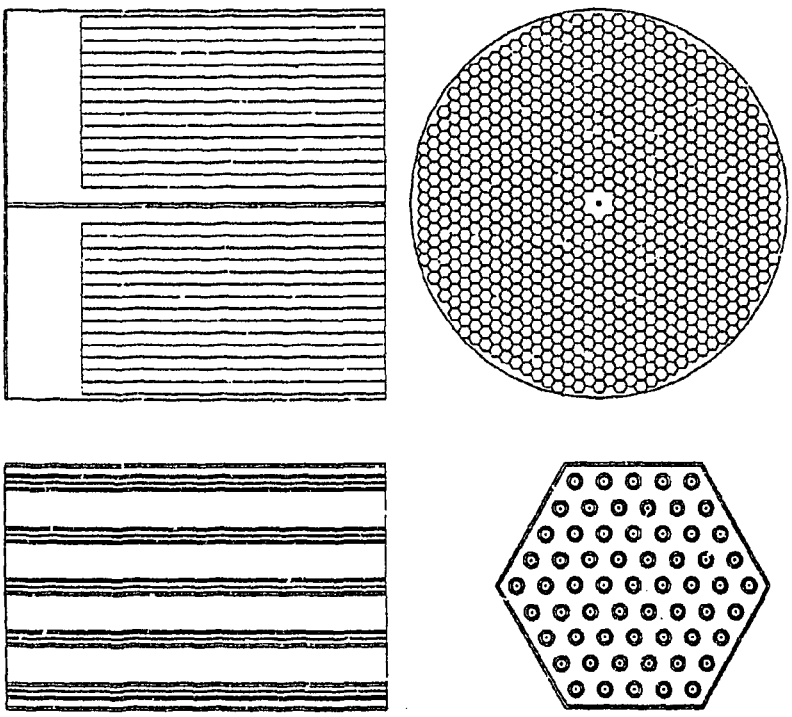

Fig. 4. Version 3. At the top part of the figure there are longitudinal section and cross-section of the prototype. At the bottom part of the figure there are longitudinal section and cross-section of the cell.

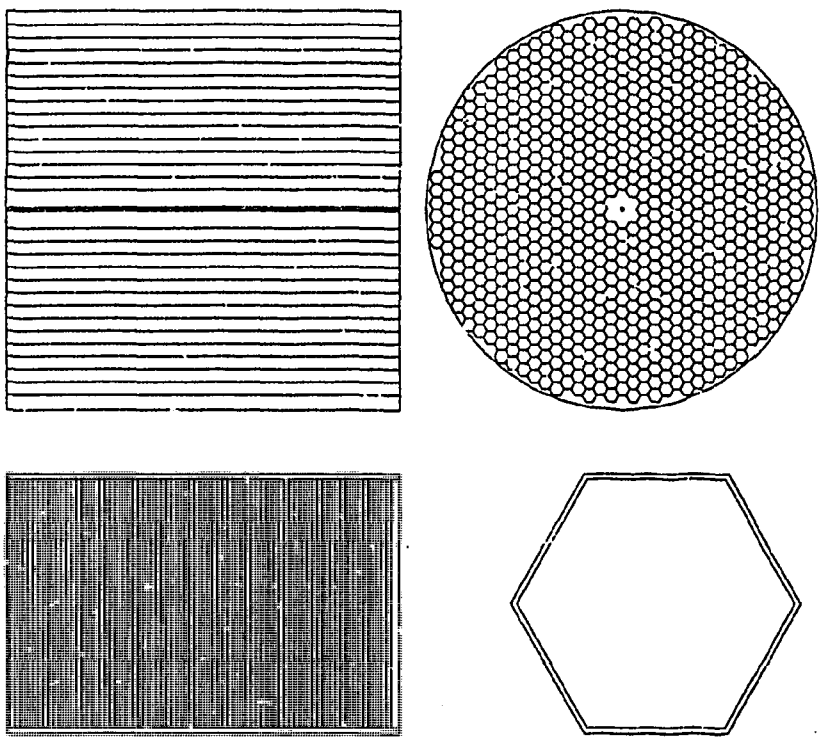

Fig. 5. Version 4. At the top part of the figure there are longitudinal section and cross-section of the prototype. At the bottom part of the figure there are longitudinal section and cross-section of the cell.

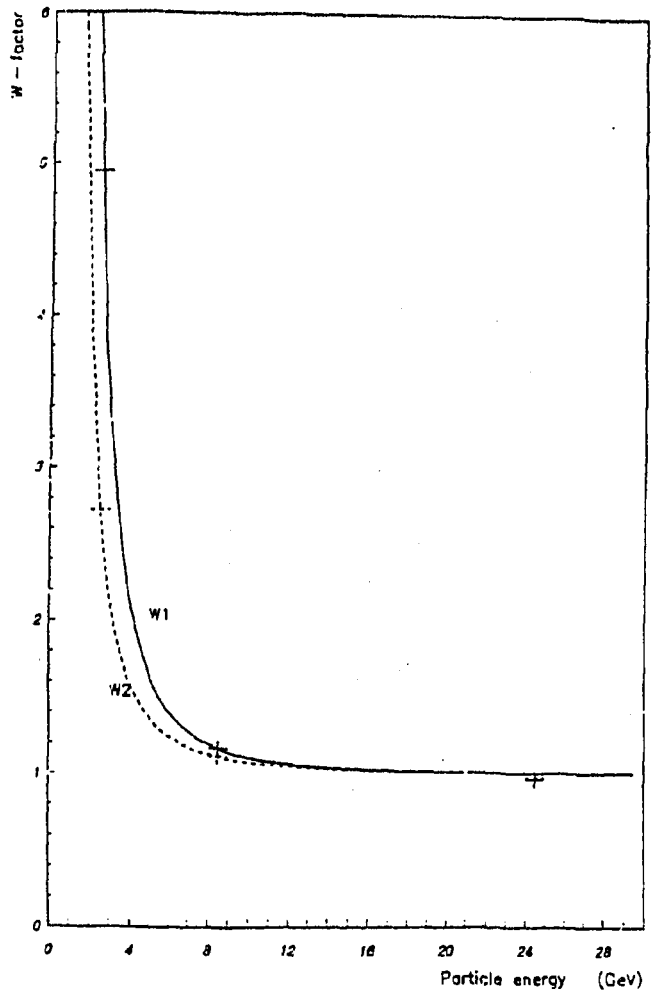

Fig. 6. Dependence of the weighted coefficients W1 and W2 on the pions energy for first and second sections of calorimeter version 4. The coefficients values are obtained from the minimization procedure of functional (2).

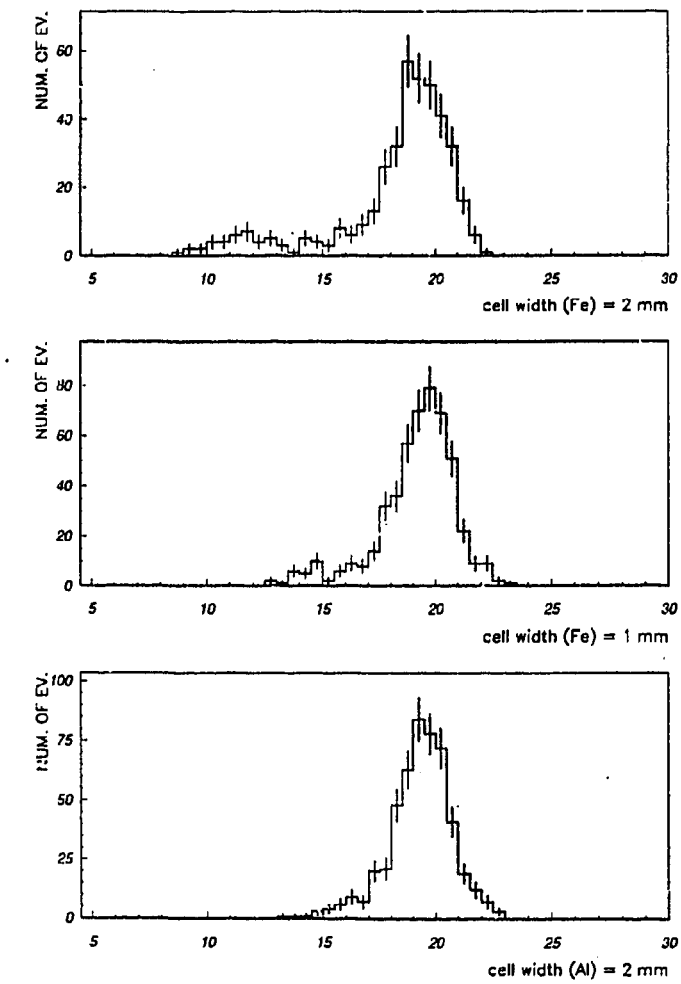

Fig. 7. Examples of the amplitude distributions for E=25 GeV electrons for the cases, when the material type and the wall thickness are varied.

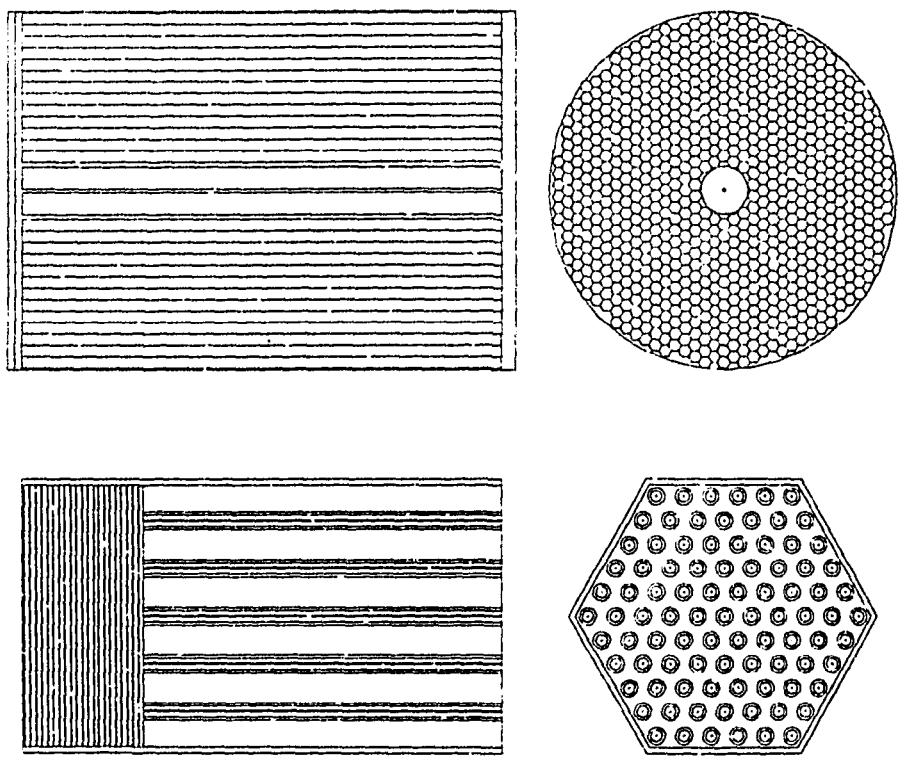

Fig. 8. Version 5. At the top part of the figure there are longitudinal section and cross-section of the prototype. At the bottom part of the figure there are longitudinal section and cross-section of the cell.

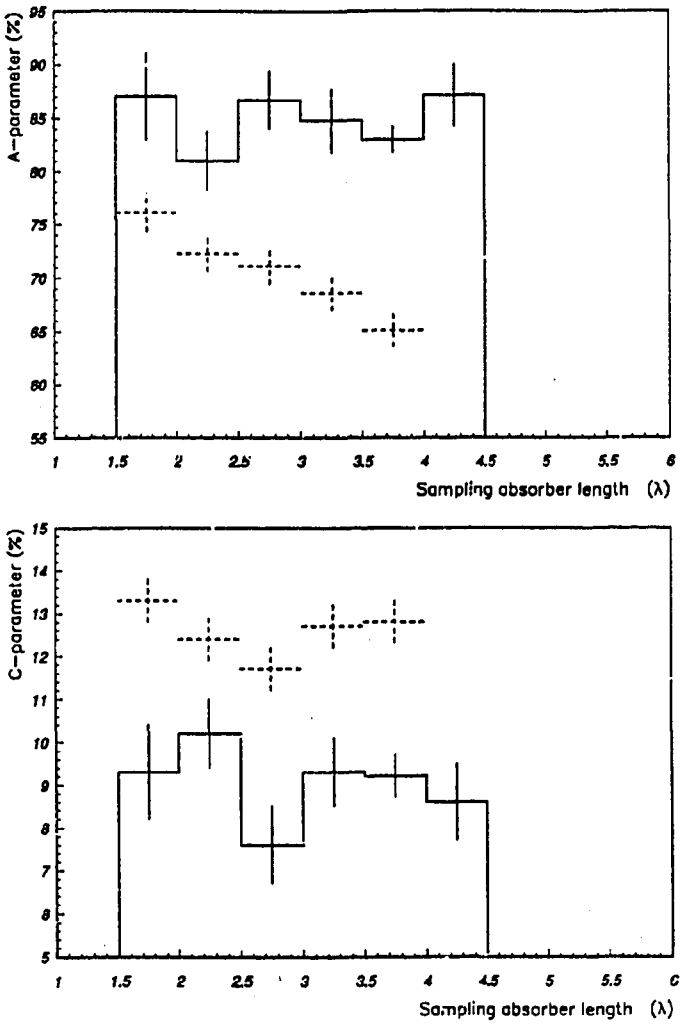

Fig. 9. Hybrid calorimeter. Dependence of the energy resolution parameters A and C from expression (1) on the length of the cell layered section. Solid line - lead absorber in the full volume of a cell and 127 tubes in each cell. Dotted line - iron absorber plates in the first cell section and 91 tubes in each cell.

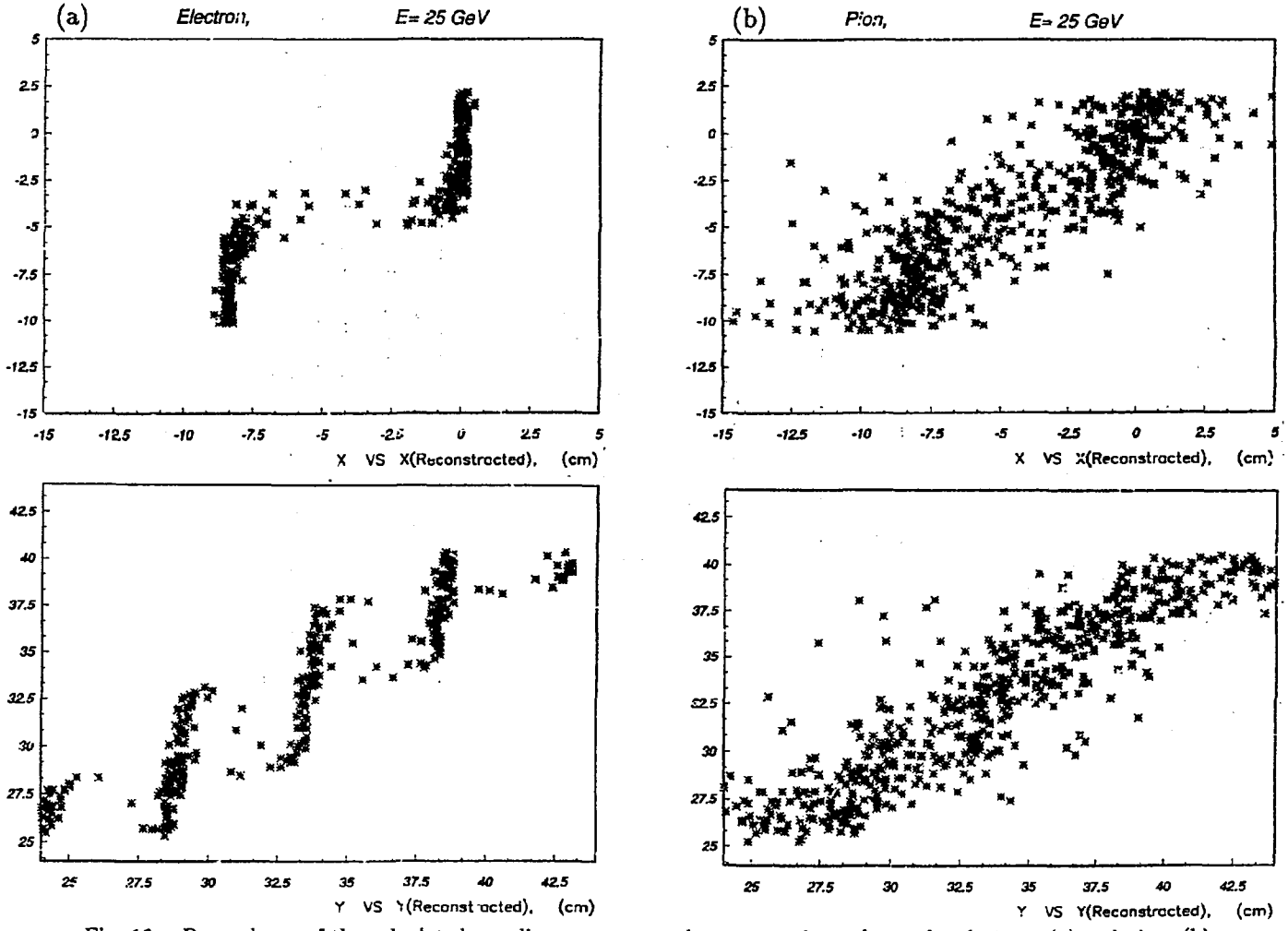

Fig. 10. Dependence of the calculated coordinates $< x >$ and $< y >$ on the real ones for electrons (a) and pions (b).

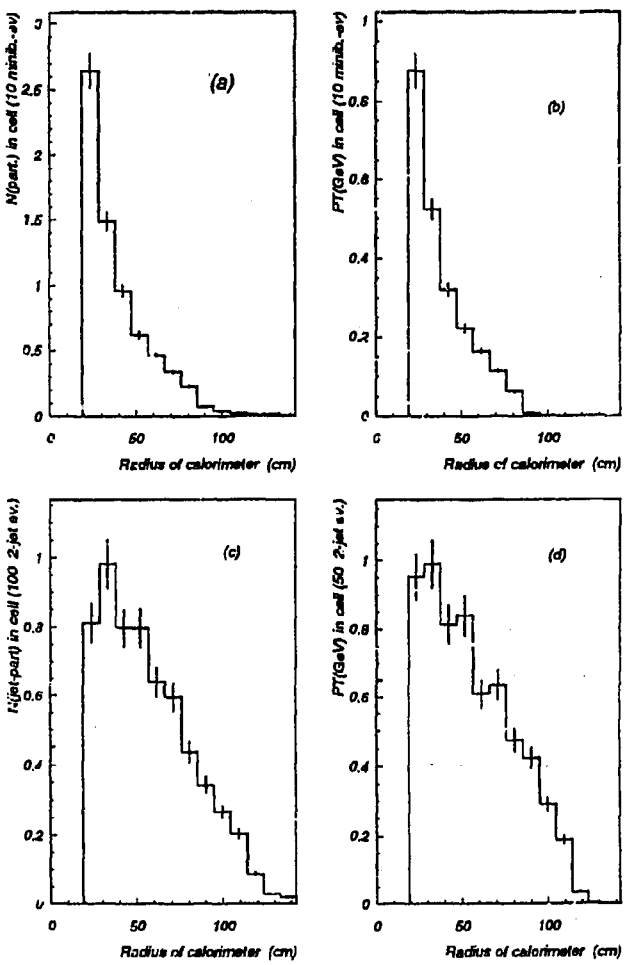

Fig. 11. Comparison of 2-jet and MINIBIAS events. (a)- number of the incoming particles in the cells along the calorimeter radius R for 10 MINIBIAS events; (c)- the same for the jet particles for 100 2-jets events; (b)- the mean value of P_T for the incoming particles in the cells along the calorimeter radius R for 10 MINIBIAS events; (d)- the same for the jet particles for 50 2-jets events.

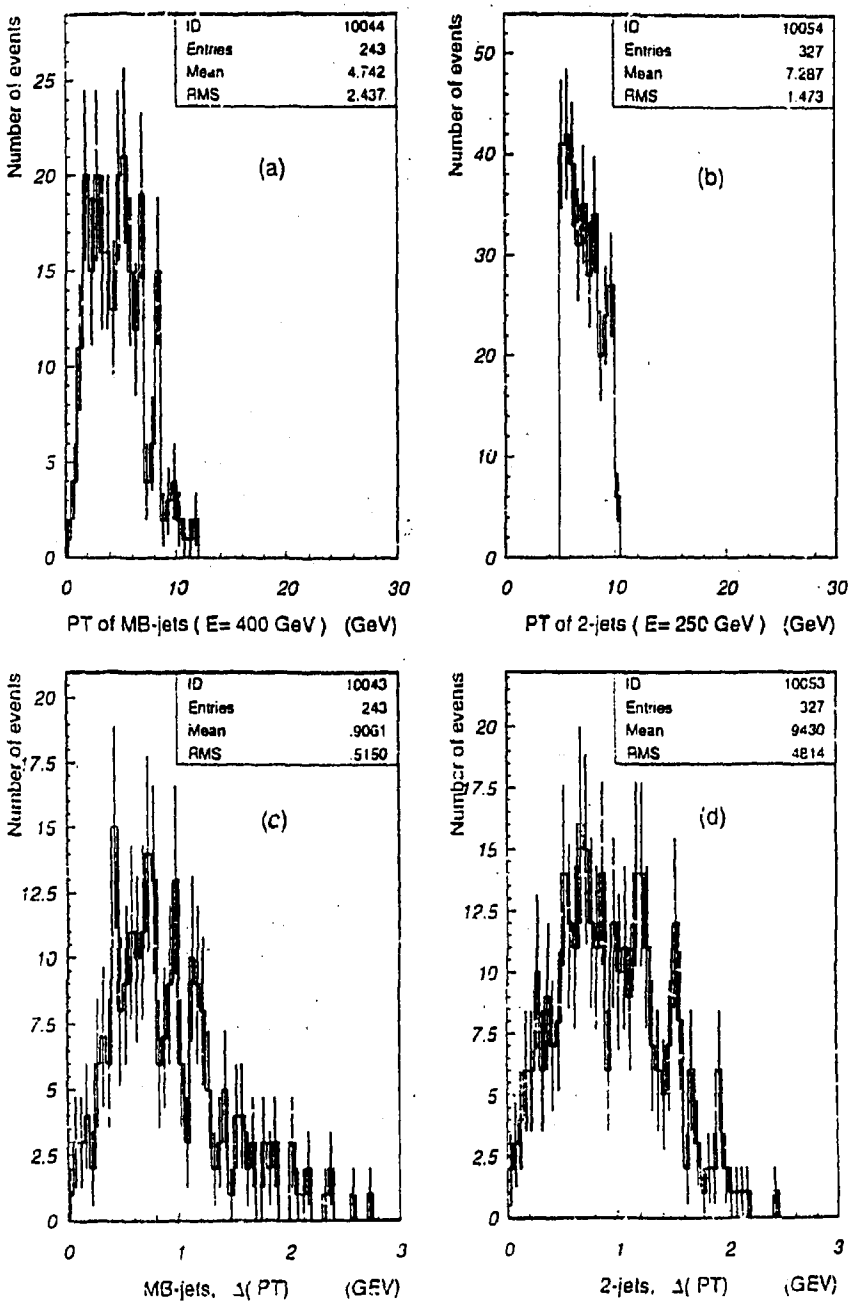

Fig. 12. Distributions of $P_T(jet)$ values and detected $|\Delta\vec{P}_T|$ values for MINIBIAS jets (a,c) and for jets from 2-jets events (b,d).

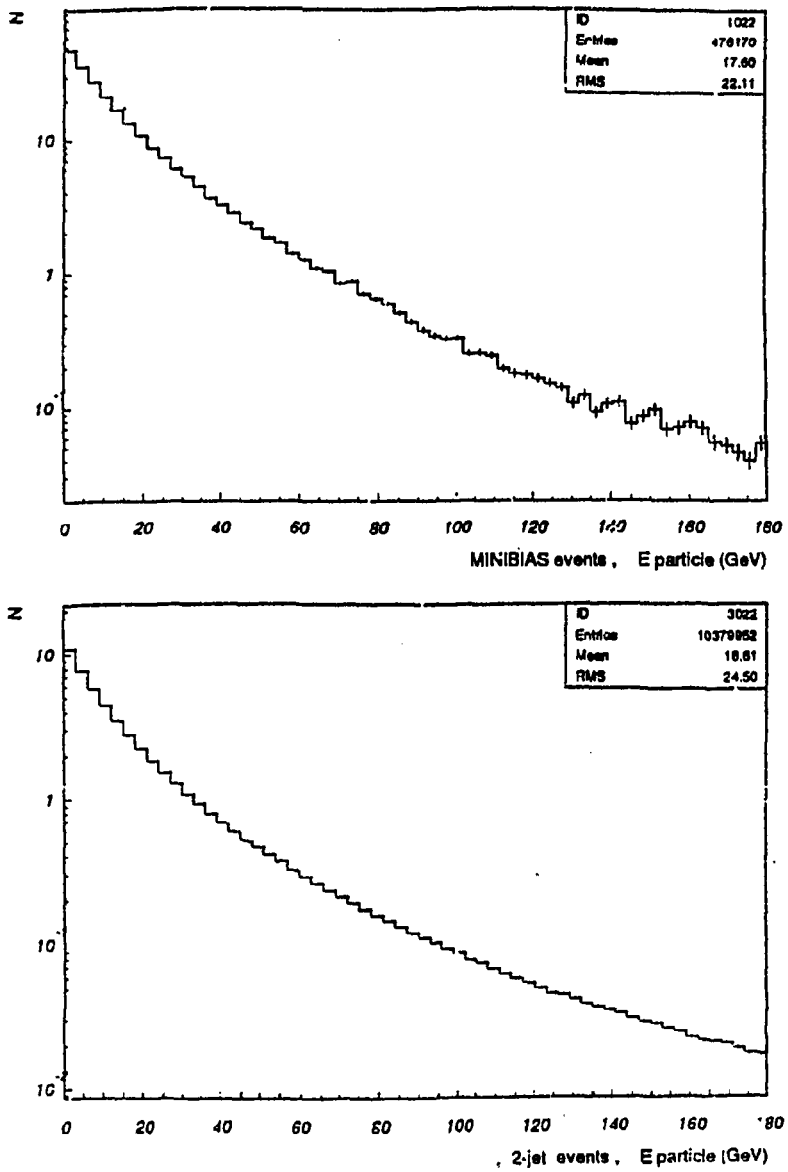

Fig. 13. Energy distributions of the incoming particles in the forward calorimeter for 2-jet (P_T >40 GeV) and MINiBIAS events.

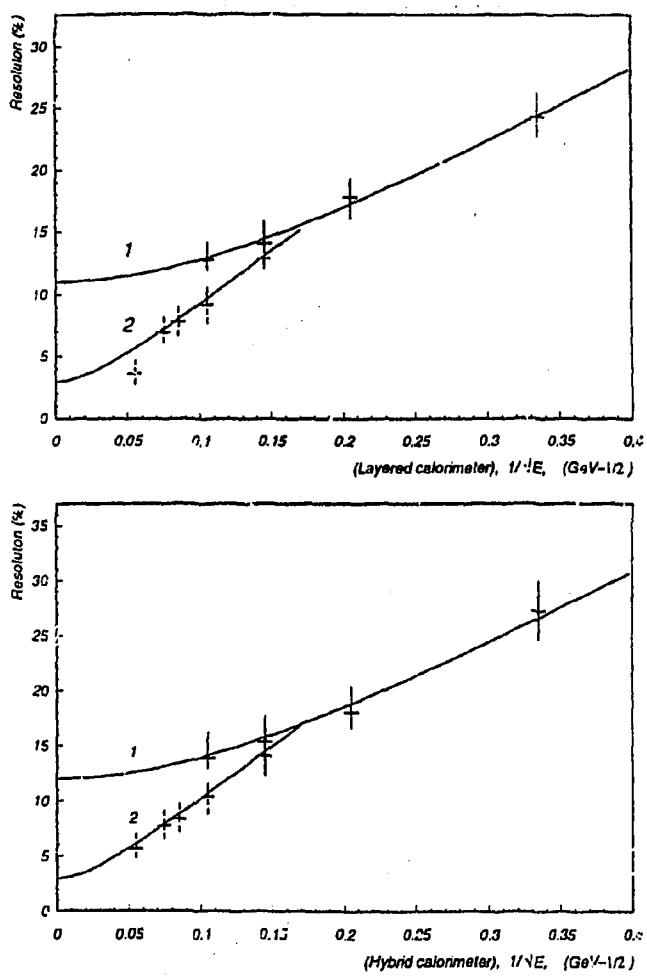

Fig. 14. Energy resolution for a single pion (curve 1) and for MINIBIAS jets (curve 2) for the layered calorimeter version and for the hybrid one.

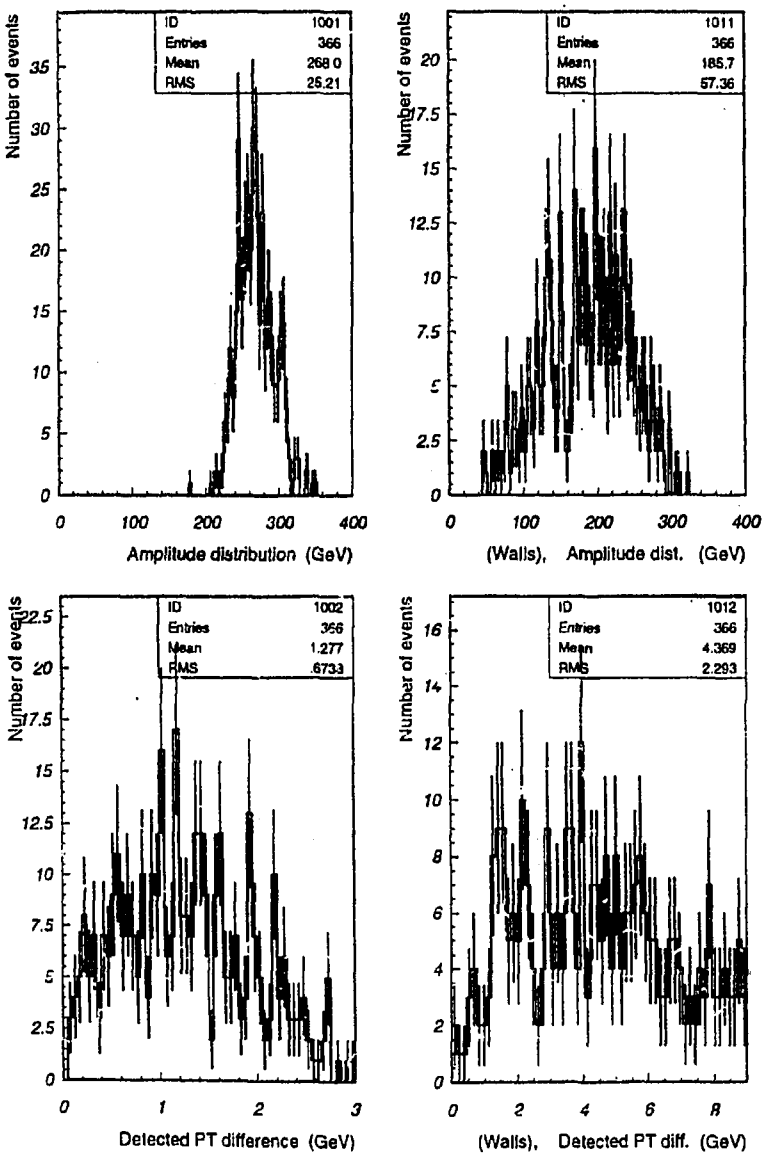

Fig. 15. Amplitude distributions and detected $|\Delta\vec{P}_T|$ distributions for jets with the energy $E_j = 250$ GeV. The left part of the figure is obtained without the presence of the criostat system. The right part of the figure is obtained in the presence of the criostat system situated before the forward calorimeter (see Appendix 2).

References

[1] Didak F. and Jenni P. (spokespersons);
Letter of Intent, CERN/LHCC/92-4, 1992.

[2] Batalov A.A. et al., EAGLE Int.Note, CAL-NO-10, 1992;
Babintsev V.V. et al., ATLAS Note, CAL-NO-028, 1993.

[3] Batalov A.A at al. IHEP 92-102,1992, Protvino (in Russian);
Batalov A.A at al. IHEP 92-140,1992, Protvino (in Russian);
Konstantinov V.F. et al. ATLAS Note. CAL-NO-027, 1993.

[4] Denisov S. et al. Nucl. Instr. and Meth., A335 (1993) 106.

[5] Baintsev V.V. IHEP 92-20, 1992, Protvino (in Russian);
Babintsev V.V. EAGLE Internal note, CAL-NO-007, 1992;
Babintsev V.V. IHEP Preprint 92-164, 1992, Protvino.

[6] Brun B. et al. CERN DD/EE/84-1 (1987).

[7] Babintsev V.V. IHEP Preprint 93-73, 1993, Protvino.

[8] Aubert B. et al. Nucl. Instr. and Meth., A334 (1993) 383.

[9] Akopdjanov G.A. et al IHEP 76-110, Protvino, 1976;
Akopdjanov G.A. et al. Nucl. Instr. and Meth., 140 (1977) 441;
Donskov S.E. et al. IHEP 76-109, Serpukhov, 1976;
Bushnin U.B. et al. IHEP 74-24, Serpukhov, 1974;
Binon F. et al. Nucl. Instr. and Meth., 188 (1981) 507;
Binon F. et al. Nucl. Instr. and Meth., A248 (1986) 86;
Behrens U. et al. Nucl. Instr. and Meth., A289 (1990) 115;
De Angelis A. et al. Nucl. Instr. and Meth., A287 (1990) 397;
Abachi S. et al. Nucl. Instr. and Meth., A324 (1993) 53;
Aubert B. et al. Preprint CERN-PPE/91-73, 1991.

[10] Bengtsson H.-U. et al. Computer Physics Commun. 46(1987)43.

[11] "Large Hadron Collider Workshop". Proceedings vol. II, ed. G.Jarlskog,
D.Rein, CERN 90-10, ECFA 90-133.

[12] C.W.Fabjan. Prepint CERN-PPE/93-124, 1993.

[13] Galactionov Yu. et al. Nucl. Instr. and Meth., 251 (1986) 258.

Received March 2, 1994

Appendix 1

The simulated data obtained with the help of the GEANT3.15 code have been compared with the experimental ones with the aim to fix the GEANT parameter values for the simulation purpose. The experimental data from the electromagnetic gas ionization prototype with the energy of the beam electrons E= 25 GeV were used. The calorimeter had the form of a tube with the radius R= 5 cm filled with the lead absorber plates 0.55 cm thick. The thickness of the gas gaps between the absorber plates is 0.24 cm. The total length of the prototype is 30 cm. The gas mixture ($90\%Ar + 10\%CF_4$) was pumped into the prototype under the pressure of P= 30 atm. There were used two sets of parameter values for the program GEANT3.15. They are presented in fig.1. For the first set of the parameters the simulated energy resolution equals (4.6±1.3)%, for the second one - (3.9±1.0)% (fig.1b). The experimental energy resolution equals 4.0%. Hence, both sets of parameter values give a contented description of the experiment although the second parameter set gives much more time consuming process as compared with the first one.

Other experimental results were taken for the following two hadron calorimeters. The first one (L3 experiment[13]) has the uranium absorber plates 4.5 mm thick with 6 mm gaps. The total length of the calorimeter is 5 interaction lengths. Proportional chambers are filled with the gas mixture ($80\%Ar + 20\%CO_2$) under the pressure 1 atm. The energy of incoming particles is 6 GeV. The second calorimeter is a high pressure gas ionization sampling calorimeter[4]. The uranium absorber plates in the first section of the calorimeter were covered by aluminium clads. The thickness of the uranium plates is 6.5 mm and for the aluminium ones they are of 1.5 mm and 3.5 mm. Iron absorber plates for the second section of the calorimeter were used. The total length of the hadron calorimeter is about 6 λ. The gas mixture ($95\%Ar + 5\%CF_4$) filles the gas ionization chambers under the pressure P= 30 atm. The energy of particles was E= 20 GeV. The comparison of experimental data and simulated ones is presented in table 1 for different parameters of the GEANT3.15 code. From the table it follows that FLUKA (HADR=4) does not describe the energy resolution for hadrons in the gas calorimeters.

Therefore for the simulation purpose the first set of parameter values (fig.1a) will be used in the article.

Appendix 2

Before the forward calorimeter in the ATLAS set-up there is an ENDCAP calorimeter situated in the cryostat system. This cryostat system can absorb a great amount of the particle energy before they enter the forward calorimeter. To check the influence of the cryostat system on the energy resolution of the forward calorimeter the following cryostat geometry was simulated (the private communication). The inner radius of the ENDCAP cryostat is 26 cm. This system is situated between 3.4 m and 6 m along the Z-axis from the central point of the ATLAS set-up. All particles which enter the forward calorimeter at the radius greater than 70 cm ($\theta = 2.5^0$) go through the cryostat system and pass about 1λ of the passive material. The acceptance limit of the ENDCAP hadronic module is $\theta = 4.7^0$ (R= 126 cm).

The number of jets with the energy $E_j = 250$ GeV and $P_T(jet) = 11 \pm 1$ GeV/c was generated. The jet axis was oriented in such a way that half of jet particles passed through the cryostat system. The following results were obtained after the simulation. The jet energy resolution in the forward calorimeter without the cryostat system is $R = (7.7 \pm 2.1)\%$, but with the presence of the cryostat system the jet energy resolution in the forward calorimeter equals $R = (31.1 \pm 7.8)\%$.

The measured $|\Delta\vec{P}_T| = |\vec{P}_T(jet) - \vec{P}_T^{\,meas}(jet)|$ difference for jets without the cryostat system has the average value 1.3 GeV/c with the dispersion of the $|\Delta\vec{P}_T|$ distribution 0.7 GeV. With the presence of the cryostat system these values are enlarged by the factor of 4. The amplitude distributions and measured $|\Delta\vec{P}_T|$ difference distributions are given in fig.15.

В.В.Бабинцев и др.
Некоторые варианты газового переднего калориметра.

Оригинал-макет подготовлен с помощью системы LaTeX.
Редактор А.А.Антипова. Технический редактор Н.В.Орлова.
Корректор Е.Н.Горина.

Подписано к печати 03.03.1994 г. Формат 60 × 90/16.
Офсетная печать. Печ.л. 2.25. Уч.-изд.л. 2.68. Тираж 240. Заказ 1097.
Индекс 3649. Цена 360 руб. ЛР №020498 06.04.1992.

Институт физики высоких энергий, 142284, Протвино Московской обл.

360 руб. Индекс 3649

ПРЕПРИНТ 94-24, ИФВЭ, 1994